

The local atomic structures of liquid CO at 3.6 GPa and polymerized CO at 0 to 30 GPa from high pressure pair distribution function analysis

Nadine Rademacher^{*a}, Lkhamsuren Bayarjargal^a, Wolfgang Morgenroth^a,
Björn Winkler^a, Jennifer Ciezak-Jenkins^b, Iskander G. Batyrev^b
and Victor Milman^c

^aInstitut für Geowissenschaften, Goethe-Universität Frankfurt,
60438 Frankfurt am Main, Germany

^bUS Army Research Laboratory, RDRL-WML-B (Bldg. 390),
Aberdeen Proving Ground, MD 21005, United States

^cAccelrys, 334 Science Park, Cambridge CB4 0WN, United Kingdom

*Email: Rademacher@kristall.uni-frankfurt.de

Keywords: high-pressure react., liquids, polymerization, pair distribution function, CO

Abstract

The local atomic structures of liquid and polymerized CO and its decomposition products have been analyzed at pressures up to 30 GPa in diamond anvil cells by X-ray diffraction, pair distribution function (PDF) analysis, single-crystal diffraction and Raman spectroscopy. The structural models were obtained by density functional theory (DFT) calculations. The analysis of the PDF of a liquid CO-rich phase revealed that the local structure has a pronounced short-range order. The PDFs of polymerized amorphous CO measured at several pressures revealed the compression of the molecular structure. The lengths of the covalent bonds did not change significantly with pressure. The experimental PDFs could be reproduced with simulations from DFT-optimized structural models. This confirmed that likely structural features of polymerized CO are 4- to 6-membered rings (lactones, cyclic ethers, rings decorated with carbonyl groups) and long bent chains with carbonyl groups and bridging atoms. Laser heating at pressures of 7 to 9 GPa polymerized CO, and pressure increase to 20 GPa resulted in the formation of CO₂.

1 Introduction

Polymerization reactions of small low- Z molecules, such as N_2 , CO_2 , CO , have been of considerable interest, because of the interesting chemical, physical and mechanical properties of the reaction products.^[1;2] However, to date, very few of these polymers have been quenched to ambient^[3;4] or near-ambient^[5] conditions.

A phase transformation from molecular CO to a polymer was first observed three decades ago during Raman spectroscopic experiments at pressures near 5 GPa and ambient temperature^[6]. Subsequent single crystal X-ray diffraction experiments conducted at similar conditions revealed diffraction features consistent with an amorphous material^[7]. It was demonstrated that the polymeric CO , or p- CO as the phase became commonly known, could be quenched to ambient conditions and that it was stable in air for months.^[6] Since these earlier reports, the chemical structure^[3;4;6-10], photochemical response^[3;4;8;10], as well as the pressure-induced reactivity and kinetics of transition^[4] of p- CO have been experimentally studied. Utilizing a combination of solid-state MAS ^{13}C NMR, FT-IR, and mass spectroscopy, the structure of the random polymer network has been inferred to consist of lactone-like carbonyls and chains with conjugated $C=C$ bonds^[3]. Such structures can easily liberate CO_2 , which was shown to be a primary decomposition product, to form graphitic layers^[3]. Additionally, the high-pressure behavior of carbon monoxide was found to be strongly influenced by the wavelength of irradiation. The transition pressure at which molecular CO transforms to p- CO was nearly 1 GPa less when visible light was used as opposed to infrared radiation^[3]. Quenched p- CO reacts violently when irradiated with a YAG laser at relatively low power (<100 mW), which led to the suggestion that p- CO is a material with high energy density^[3]. Subsequent differential scanning calorimetric experiments yielded an energy release between 1 to 8 kJ/g, whereas conventional energetic materials have thermal energy contents between 1 to 3 kJ/g^[3]. Depending on the synthesis and processing conditions, quenched p- CO exhibits a broad range of color, morphology and metastability, which has hampered more definitive structural determination and characterization of its fundamental properties.

Liquid CO has previously been studied by neutron diffraction at low temperatures and elevated pressures by Howe et al.^[11]; Bellissent-Funel et al.^[12] and most recently by Temleitner and Pusztai^[13] in order to understand the structure and the orientational correlations of the liquid. The position of the first and most intense feature in the structure function has been observed at about 1.9 \AA^{-1} at 83.5(2) K and $4.2(2) \cdot 10^{-4}$ GPa^[12]. Distances between 3.8 to 7.2 \AA to nearest neighbors in liquid CO have been obtained from radial distribution functions. While Howe et al.^[11]; Bellissent-Funel et al.^[12] have found no evidence for a preferred orientation of the CO molecules within the liquid, the modeling results by Temleitner and Pusztai^[13] indicated that well defined orientational correlations are present in liquid CO .

Total scattering techniques have proven to be a powerful tool for the determination of accurate structural parameters of crystalline as well as disordered, amorphous and nanocrystalline materials^[14;15] at ambient and high pressures^[16;17]. The pair distribution function (PDF, $G(r)$) gives the probability of finding atoms separated by a distance r . $G(r)$ is experimentally obtained by a Fourier transform of the corrected and normalized diffraction data, $S(Q)$:

$$G(r) = 4\pi r [\rho(r) - \rho_0] = \frac{2}{\pi} \int_0^{\infty} Q [S(Q) - 1] \sin(Qr) dQ \quad (1)$$

$\rho(r)$ is the microscopic pair density, ρ_0 is the average number density, $S(Q)$ is the total scattering structure function and Q is the magnitude of the scattering vector, which is given by $Q = 4\pi \sin \theta / \lambda$ with θ being the scattering angle and λ the wavelength of the radiation. Detailed information on the procedures can be found in Egami and Billinge^[18]. *In situ* PDF studies at high pressure in diamond anvil cells (DAC) are challenging, because the set-up of DAC experiments in principle does not fulfill the requirements for high-quality PDF data, such as access to large scattering angles and high signal-to-background ratios^[16].

In the present study, experimental measurements, coupled with quantum chemical modeling, have been used to derive new information regarding the structure of a liquid CO-rich phase, amorphous p-CO both at high pressure up to 30 GPa and quenched to ambient conditions as well as the decomposition products of p-CO.

2 Computational details

2.1 Liquid CO

The structural models for liquid CO were obtained by density functional theory (DFT^[19]) using the program *CASTEP*^[20]. We used the PBEsol generalized gradient approximation^[21], “on the fly” pseudopotentials from the *CASTEP* database, a plane waves basis set with an energy cut-off of 610 eV and a $6 \times 6 \times 6$ Monkhorst-Pack^[22] grid.

The models were constructed from the known structures of crystalline α - and ϵ -CO phases^[9]. α -CO crystallizes in space group $P2_13$ with 4 molecules per unit cell^[23] and ϵ -CO crystallizes in space group $R3c$ with 24 molecules per unit cell^[9].

2.2 Polymerization of CO

The models for the p-CO structures were obtained through relaxation of lattice vectors and atomic positions using the Quickstep/CP2k package (version 2.3)^[24] with a Gaussian and plane wave basis sets, which describe wave functions around atoms and interstitial space respectively. The DZVP-GTH (Goedecker-Teter-Hutter^[25;26]) basis set was used. The pseudo potentials within the PBE approximation of GTH-PBE-q4 for carbon, GTH-PBE-q6 for oxygen, and GTH-PBE-q2 for He atoms were employed. For all plane wave calculations, a cut-off energy of 800 eV was applied. In order to achieve convergence of structural relaxation of molecular crystals at low pressures, DFT-D3 dispersion corrections were applied^[27]. The simulations were started by the construction of the disordered cubic δ -phase of solid CO, which was based on experimental crystallographic data previously discussed^[9]. The space group was $P1$. Two different supercells with 128 and 432 atoms were used. The unit cell was then compressed at the various pressures starting from 3 GPa to 18 GPa in 1 GPa increments. Further simulations with 128 atom models were started from the δ -phase which had 12.5 % He atoms, because our experiments were performed with CO-He mixtures and it was expected that He was dissolved within the CO.

3 Results

3.1 Computation

The atomistic model calculations served as a basis for the refinement of X-ray data. Hence, the reliability of the model calculations was first established by comparison to experimental data. The unit cell parameters of the starting models and DFT-optimized structures are summarized in table 1. The DFT-optimized structures of α - and ϵ -CO as well as the original ϵ -CO structure are presented in figure 1. The DFT optimization reproduced the lattice parameters of the experimental structure of the ϵ -phase at 5.5 GPa very well. The discrepancy was 1 %. Therefore, we used the DFT structures obtained at 3.6 GPa as extrapolated models of liquid CO for the PDF simulations at this pressure.

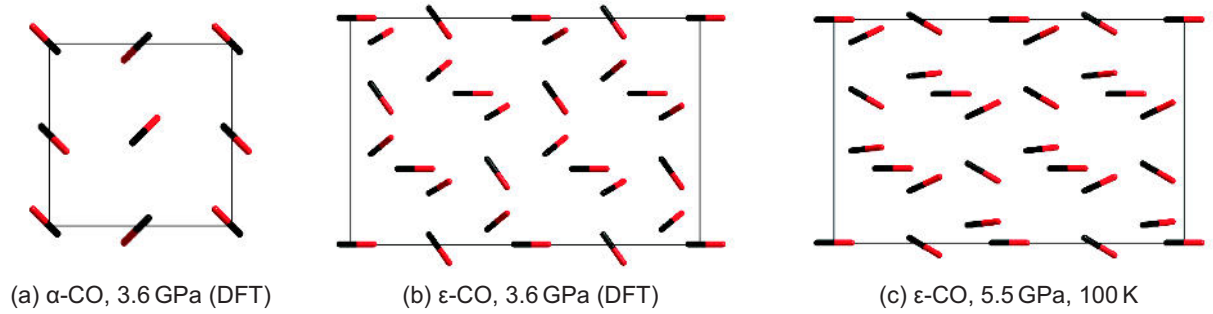


Figure 1: a) DFT-optimized crystal structure of α -CO at 3.6 GPa (view along a). b) DFT-optimized structure of ϵ -CO at 3.6 GPa (view along a). c) Crystal structure of ϵ -CO at 5.5 GPa and 100 K as determined by Mills et al.^[9] (view along a). C atoms are drawn black and O atoms red.

Phase	p/GPa	T/K	Space group	Z	$a/\text{\AA}$	$c/\text{\AA}$	$V/\text{\AA}^3$
ϵ -CO ^[9]	5.5	100	$R3c$	24	8.244	11.25	662.2
ϵ -CO, DFT optimized	5.5	0	$R3c$	24	8.234	11.153	655
ϵ -CO, DFT optimized	3.6	0	$R3c$	24	8.5155	11.4186	717.1
α -CO ^[23]	0	20	$P2_13$	4	5.63	—	178.5
α -CO, DFT optimized	3.6	0	$P2_13$	4	4.9339	—	120.1

Table 1: Comparison of experimentally determined lattice parameters of CO polymorphs to the results of DFT-based model calculations.

We then investigated whether a DFT-based model would reproduce a pressure induced polymerization. To identify the polymerization, we determined the largest distance between two atoms for which a bond may be formed as the ideal bond length increased by 15 % (defined as the sum of the covalent radii of the two atoms forming the bond), i.e. polymerization occurred if the C–C bond length was in the range of 1.518 to 1.557 \AA for the lactones, the C–O bond in the range of 1.393 to 1.454 \AA in lactones and the C=O bond length in carbonyl groups around 1.207 \AA . The C \equiv O bond length in a CO molecule not yet incorporated in the network was 1.128 \AA .

In our model calculations, the formation of a random network from isolated CO molecules began near 7 GPa for the 432 atom and at 8 GPa for 128 atom models^[28]. The structures of the optimized δ -CO (432 atom model) at 3 GPa, after the onset of

polymerization at 7 GPa and after the polymerization is nearly completed at 18 GPa are presented in figure 2. The first polymerized fragments observed in both models are carbon zig-zag chains with oxygen atoms (see figure 3). Further compression to between 15 and 18 GPa resulted in an almost complete transformation of the molecular crystal phase to a random polymerized network consisting primarily of long bent carbon chains with carbonyl groups and bridging atoms (figure 3). A minor amount of the network consisted of 4-, 5-, and 6-membered rings which included cyclic ethers, lactones and rings which were decorated with carbonyl groups (figure 3). The transitions to the polymer phases were irreversible, which resulted in a hysteresis loop shown in figure 4 for the number of CO fragments that are unconnected to the network. The random structure obtained at 18 GPa remained metastable to 3 GPa upon decompression. The same type of hysteresis was observed in the mass density. The density of the polymeric phase obtained upon compression was 1.69 g/cm^3 at 7 GPa. At 18 GPa, the density increased to 2.46 g/cm^3 for the 432 atom model. Upon decompression, the density of the network obtained by lowering the pressure down to 7 GPa from 18 GPa was $\approx 2.04 \text{ g/cm}^3$, and the total energy was $\approx 2.3 \text{ eV}$ lower than that of the structure obtained by compression of the δ phase at 7 GPa.

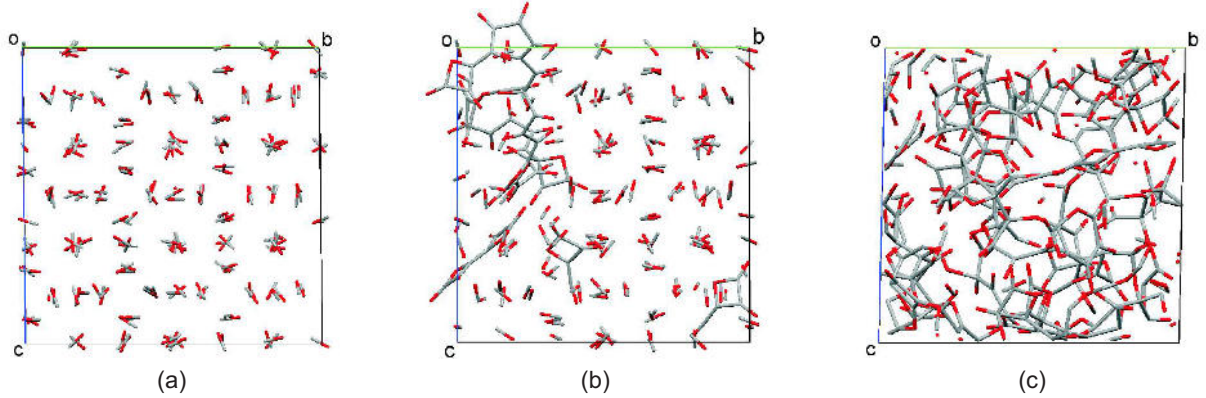


Figure 2: DFT-optimized structures of the 432 atom model of δ -CO at 3 GPa (a), 7 GPa (b) and 18 GPa (c). The polymerization began near 7 GPa and was almost completed at 18 GPa. C atoms are drawn grey and O atoms red.

The properties of the random network were modified by the introduction of He, since the experiments were performed with CO-He mixtures. The formation of the random network began at 9 GPa and by 15 GPa all CO molecules were either part of closed rings or chain-type structures. The density was 2.52 g/cm^3 at 15 GPa. From the simulations, it appeared that the He atoms facilitate the formation of the random polymeric structure at lower pressure relative to that observed in pure p-CO. Additionally, the He atoms assisted in the stabilization of the quenched structure down to 100 bar. During the decompression process the structure lost only a few CO molecules. In contrast, simulations of pure CO (without He atoms) at 100 bar showed that nearly an order of magnitude more CO units were lost during the decompression process. The analysis indicated that terminal ends of the chains not connected in rings are the weakest links and that CO units separate from the terminal ends first as the pressure is decreased.

The most important result of this work is that He atoms facilitate the formation of p-CO under isotropic compression and help to preserve the polymeric random network under lowering the pressure down to 100 bar.

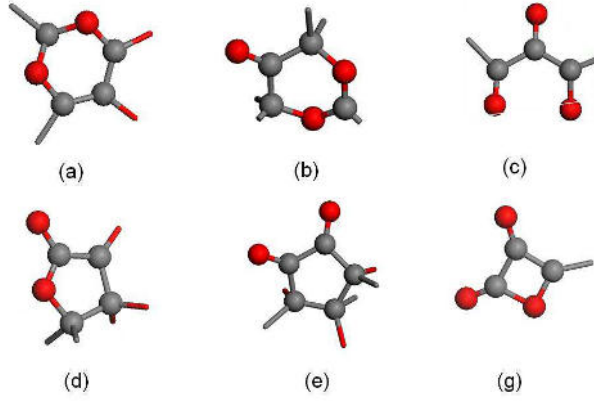


Figure 3: Typical fragments of p-CO (C: grey, O: red). Atoms with one or two unsaturated bonds are connected to other atoms in the network, atoms represented by a ball (excluding atoms within rings or chains) are terminal atoms.

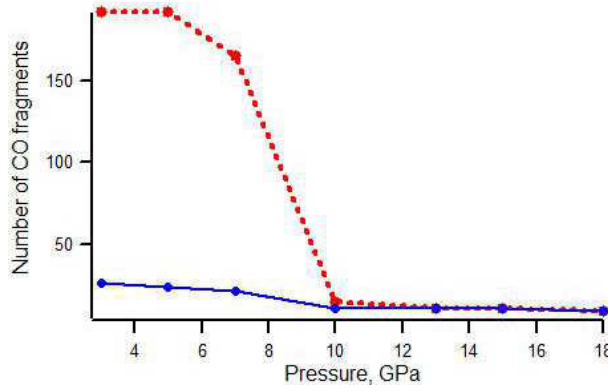


Figure 4: Number of CO molecules not connected to the p-CO network for the 432 atom model (dotted line: increasing pressure, solid line: decreasing pressure).

p/GPa	$a/\text{\AA}$	$b/\text{\AA}$	$c/\text{\AA}$	$\alpha/^\circ$	$\beta/^\circ$	$\gamma/^\circ$	$V/\text{\AA}^3$	$\rho/(\text{g}\cdot\text{cm}^{-3})$
0.01	12.836	10.799	11.034	93.521	90.517	100.513	1500.7	1.807
5	11.372	10.419	10.594	91.07	89.334	95.259	1249.7	2.169
11	10.796	10.200	10.301	89.828	89.054	93.982	1131.4	2.40
15	10.531	10.095	10.159	89.045	88.878	93.628	1077.5	2.516

Table 2: Lattice parameters and densities of the DFT-optimized p-CO structures which were used as structural models for the PDF simulations (the space group for all structures is $P1$).

3.2 The local structure of liquid CO at 3.6(2) GPa

The mixture of 25 vol% CO in He separated at 3.6(2) GPa with He forming a large bubble which was surrounded by CO. At this pressure CO was clearly a liquid, as the He bubble was able to move in the CO phase. This indicated that the phase separation was incomplete and that a significant amount of He remained dissolved in the CO. Pure CO has been reported to be solid at this pressure^[29]. Based on an image analysis, we determined the volume ratio of CO:He to be around 1:0.8. From the initial composition, a ratio of

around 1:1 is expected. Hence, we concluded that up to 20 % He remained dissolved in the CO. Figure 5 shows the sample chamber before (a) and after (b) the phase separation occurred. Due to the distinct separation of the two phases it was possible to collect diffraction data from the CO-rich phase and the He phase separately. The data of the He phase was then used as background for the PDF analysis as He is a very weak X-ray scatterer.

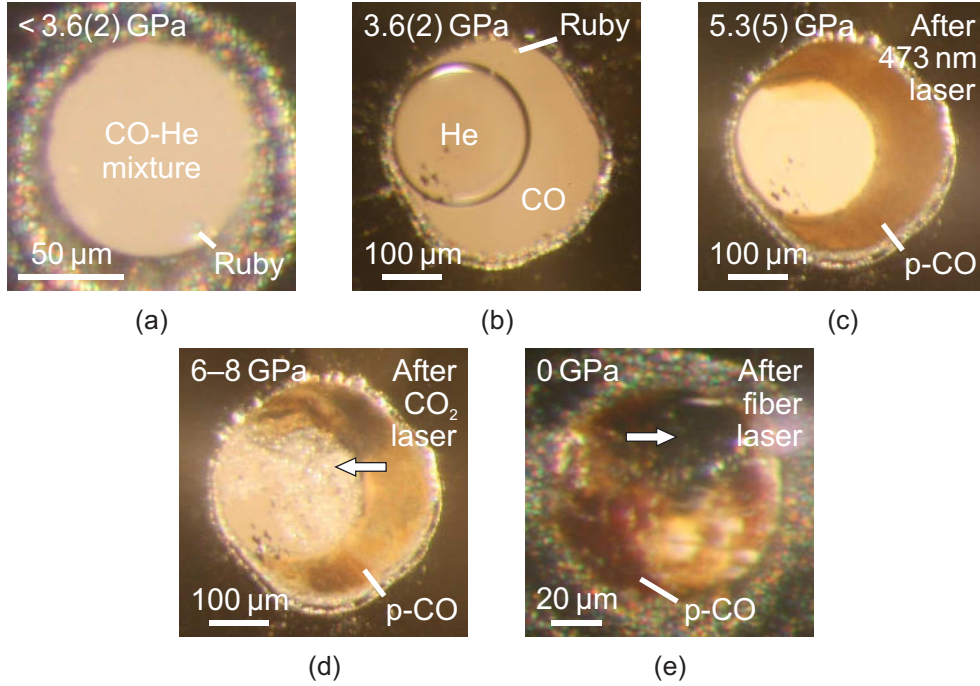


Figure 5: High pressure behavior of the 25 vol% CO-He mixture. a) The homogeneous mixture below 3.6(2) GPa. b) At 3.6(2) GPa CO and He separated with He forming a large bubble. c) Liquid CO polymerized at 5.3(5) GPa and laser irradiation yielding a red solid (p-CO). d) Laser heating of the red p-CO at 6 to 8 GPa resulted in CO₂ formation (white crystals marked by the arrow). e) Recovered sample which was laser heated at 20(2) GPa.

Figure 6 shows the integrated diffraction data of CO and He at 3.6(2) GPa and the resulting background subtracted diffraction pattern of liquid CO. Only a few broad reflections are present in the background corrected pattern. The position of the first maximum is around $2.25(1) \text{ \AA}^{-1}$.

The PDF of liquid CO as determined in our experiments is presented in figure 7. There are no structural correlations after a radial distance of about 8 \AA demonstrating the lack of long-range order. The position of the first maximum is at $1.130(5) \text{ \AA}$. This peak corresponds to the intramolecular $\text{C}\equiv\text{O}$ distance and is in excellent agreement with the literature value of 1.127 \AA obtained at a slightly larger pressure of 5.5 GPa ^[9]. The next features in the PDF and thereby the next neighbors are at around 3.5 \AA and $\approx 6 \text{ \AA}$, respectively.

In order to obtain quantitative information on the local atomic arrangement in liquid CO, the DFT-optimized structural models of CO introduced in the computation section were used to fit the experimental PDF. The comparison between the experimental PDF of liquid CO and the simulated PDFs from the structural models is presented in figure 8. The results are summarized in table 3. The simulated PDF of crystalline ϵ -CO describes

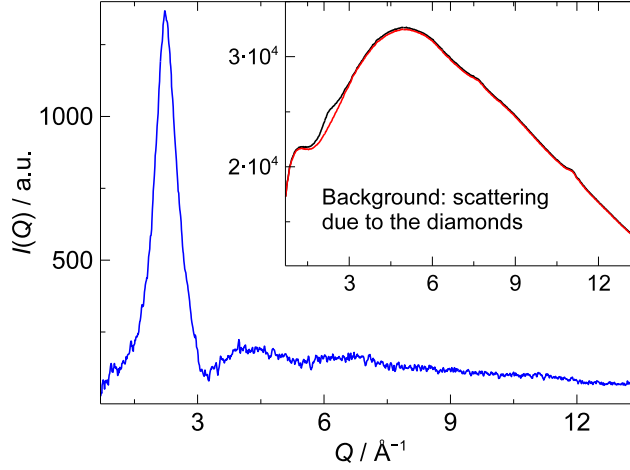


Figure 6: Integrated diffraction pattern of liquid CO at 3.6(2) GPa. The inset shows the pattern from the measurement in the CO region (black) and the He region (red). The background subtracted data (blue) shows a few broad reflections only, as expected from a liquid sample.

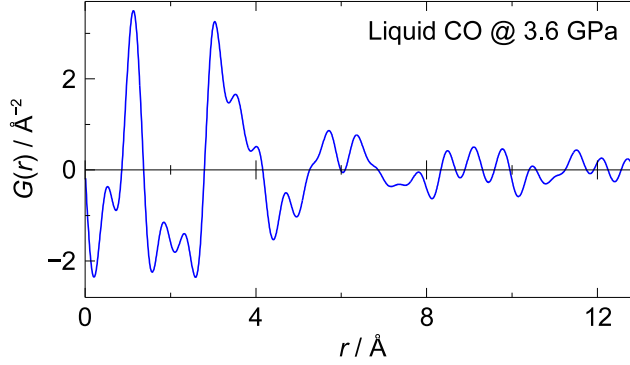


Figure 7: Experimental PDF of liquid CO at 3.6(2) GPa.

the experimental PDF of the liquid CO. The position of the first maximum at around 1.13 Å is expected to be reproduced very well, since the length of the intramolecular C≡O bond is approximately the same in the gas, liquid or solid state. But the position of the second structural peaks at around 3.5 Å is also reproduced remarkably well. This means that the second nearest neighbors in the liquid phase are as close as in these crystalline phases. A significant difference can only be seen in the peaks which are situated at around 6 Å. Here, the crystalline model underestimates the distances. Hence, the third nearest neighbors are further away in liquid CO compared to the crystalline phase. With the present data it is not possible to distinguish between the DFT-optimized, disordered δ -phase (in *P1*) and the crystalline ϵ -CO, because the simulated PDFs are very similar (see figure 8d). The important result here is, that the local structure of the liquid CO phase is characterized by strong short-range ordering and is similar to the crystalline CO analogues but very distinct from p-CO (see below).

3.3 The local structure of polymerized CO

In our experiments the polymerization of CO to the red p-CO phase was induced photochemically at 5.3(5) GPa (see figure 5c). Figure 9 shows the background subtracted

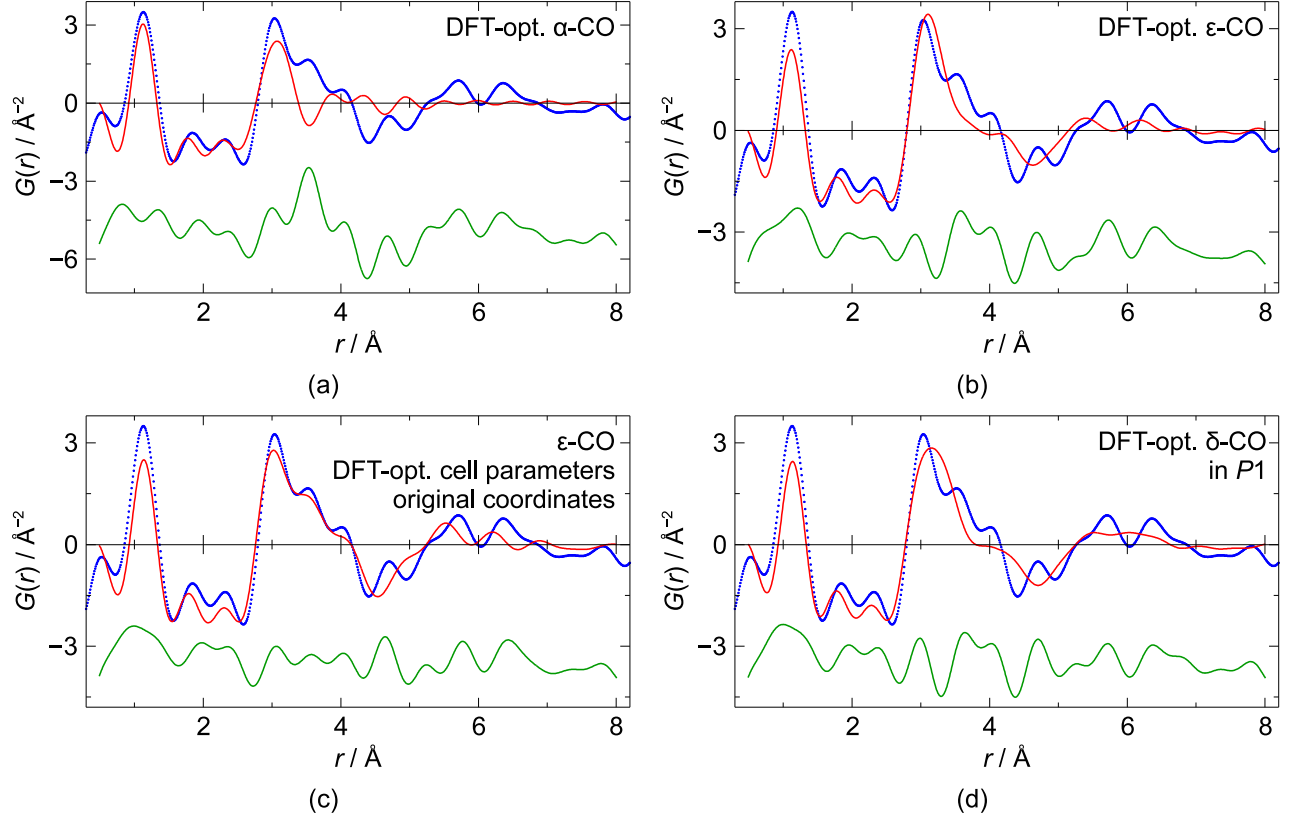


Figure 8: Refinement results for the PDF of liquid CO at 3.6(2) GPa using the DFT-optimized structures. a) α -CO at 3.6 GPa. b) ϵ -CO at 3.6 GPa. c) ϵ -CO at 3.6 GPa with unit cell from the DFT optimization and the original atomic coordinates. d) δ -CO at 3 GPa. The experimental PDF is shown as blue dotted line in each case, the calculated PDF is shown with a solid red line and the difference curve is below in green.

Model		$R_w/\%$	Scaling factor
α -CO	DFT optimized	57.0	1.9(6)
ϵ -CO	DFT optimized	38.8	1.4(4)
ϵ -CO	Atomic coordinates from Mills et al. ^[9] , cell parameters from DFT	33.2	1.5(4)
δ -CO	DFT optimized	37.6	1.4(3)

Table 3: Results of the PDF refinements of liquid CO (fit range: 0.5 to 8 Å).

diffraction patterns of liquid CO at 3.6(2) GPa, p-CO at 5.2(1), 13.9(3) and 30.2(6) GPa as well as recovered p-CO at ambient conditions. The diffraction patterns of liquid CO and p-CO differ significantly. The first reflection at around 2.3 \AA^{-1} in liquid CO shifts to higher Q values and while liquid CO has two weak reflections at 4 and 7 \AA^{-1} , respectively, p-CO only has one additional broader reflection at around 5 \AA^{-1} (in the presented region up to 8 \AA^{-1}). The first reflection in the diffraction pattern of recovered p-CO (figure 9, top) at 1.8 \AA^{-1} could be assigned to graphite. In the same region, a new reflection appeared in the diffraction pattern of p-CO at a pressure of around 24 GPa. Hence, p-CO began to decompose at around 24 GPa but it was observed up to the maximum pressure in our experiments of 30 GPa. The pressure dependence of the first strong reflection of p-CO is depicted in figure 10.

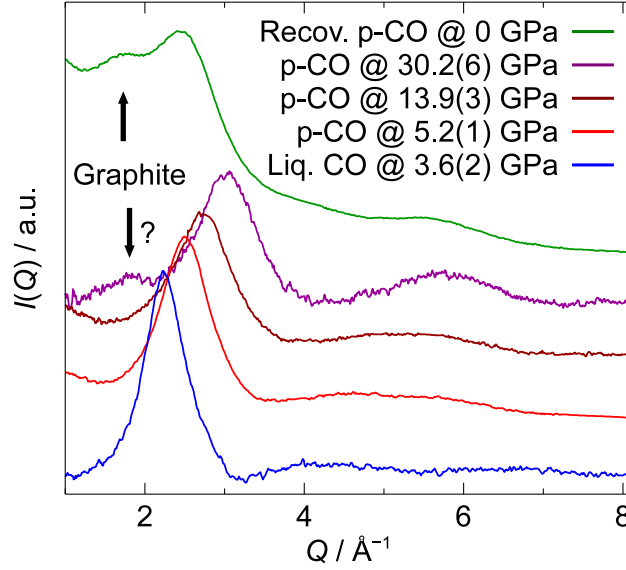


Figure 9: Background subtracted diffraction patterns of liquid CO at 3.6 GPa (bottom, blue), of p-CO at different pressures (middle, red, brown, purple) and recovered p-CO at ambient conditions (top, green). The patterns are shown with an offset in the ordinate.

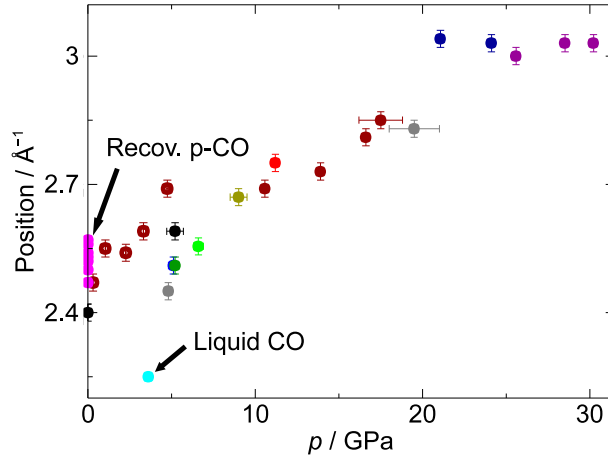


Figure 10: Pressure dependence of the position of the first reflection in the diffraction pattern of p-CO and liquid CO. Closed symbols denote data points obtained on compression and open symbols on decompression.

Figure 11 presents the pair distribution functions of liquid CO and recovered p-CO. As expected, they exhibit significant differences. The first peak at 1.1 \AA in liquid CO shifts to 1.4 \AA in recovered p-CO. This distance is a good average for C–C, C–O, C=C and C=O bonds, which are expected to be present in p-CO. Moreover, a new peak appears in p-CO at 2.4 \AA . This is a clear sign of the presence of an organic molecule larger than CO, since atom-atom distances of 2.4 \AA do not exist in CO. The structural features at around 6 \AA in liquid CO also move to smaller distances of about 5 \AA indicating the formation of the network. This demonstrates that the PDF is an excellent tool to illustrate the different atom-atom pairs in CO and the polymerized phase p-CO.

In order to obtain more information on the atomic arrangement and possible functional groups or structural fragments in p-CO, PDFs were simulated from the 128 atom models

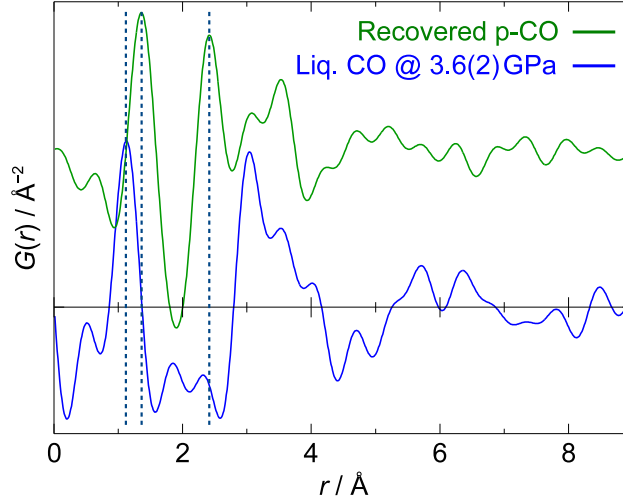


Figure 11: Experimental PDFs of liquid CO at 3.6 GPa (bottom, blue) and recovered p-CO at ambient conditions (top, green). The PDFs are shown with an offset in the ordinate. The first-neighbor peak moves from 1.13 Å in liquid CO to around 1.4 Å in p-CO and a new peak appears at around 2.4 Å indicating the formation of the extended molecular solid p-CO.

containing 12.5% He atoms and compared with the experimental data. A qualitative comparison between the simulated and experimental PDFs as well as a representative DFT-optimized model are shown in figure 12. A similar high pressure behavior of the simulated and experimental PDFs can be seen: The position of the first-neighbor peak does not change up to 15 GPa and at higher pressures it is questionable if the shift to smaller distances is meaningful or due to the insufficient data quality. The second-neighbor peak also remains at the same position but the intensity increases significantly as opposed to the third peak whose intensity decreases. The compression of the material can be seen clearly at higher r values, since the features move to smaller r values with increasing pressure.

The PDF fits using models optimized at 0.01, 5, 11 and 15 GPa are shown in figure 13 and summarized in table 4. The 0.01 GPa model was used for a comparison with quenched p-CO. As mentioned earlier, recovered p-CO consists of 2 phases, namely p-CO and graphite. The PDF fit at 0 GPa was therefore performed with these two structural models. The agreement between the simulated and experimental PDF at each pressure is excellent considering the fact that the unit cell and atomic position were not refined. Moreover, the periodic boundary conditions, which are automatically applied in *PDFgui*, can have an influence on the intensities of the PDF peaks, which might cause some differences between the experimental and simulated curves. In summary, the simulated PDFs from the structural models are consistent with our experimental data.

p/GPa (sim.)	p/GPa (exp.)	$R_w/\%$	Scaling factor
0.01	0	23.7	0.90(3) (for p-CO)
5	5.2(1)	34.3	1.1(1)
11	10.6(2)	29.6	1.1(1)
15	13.9(3)	31.9	1.0(1)

Table 4: Results of the PDF refinements of p-CO (fit range: 0.5 to 8 Å).

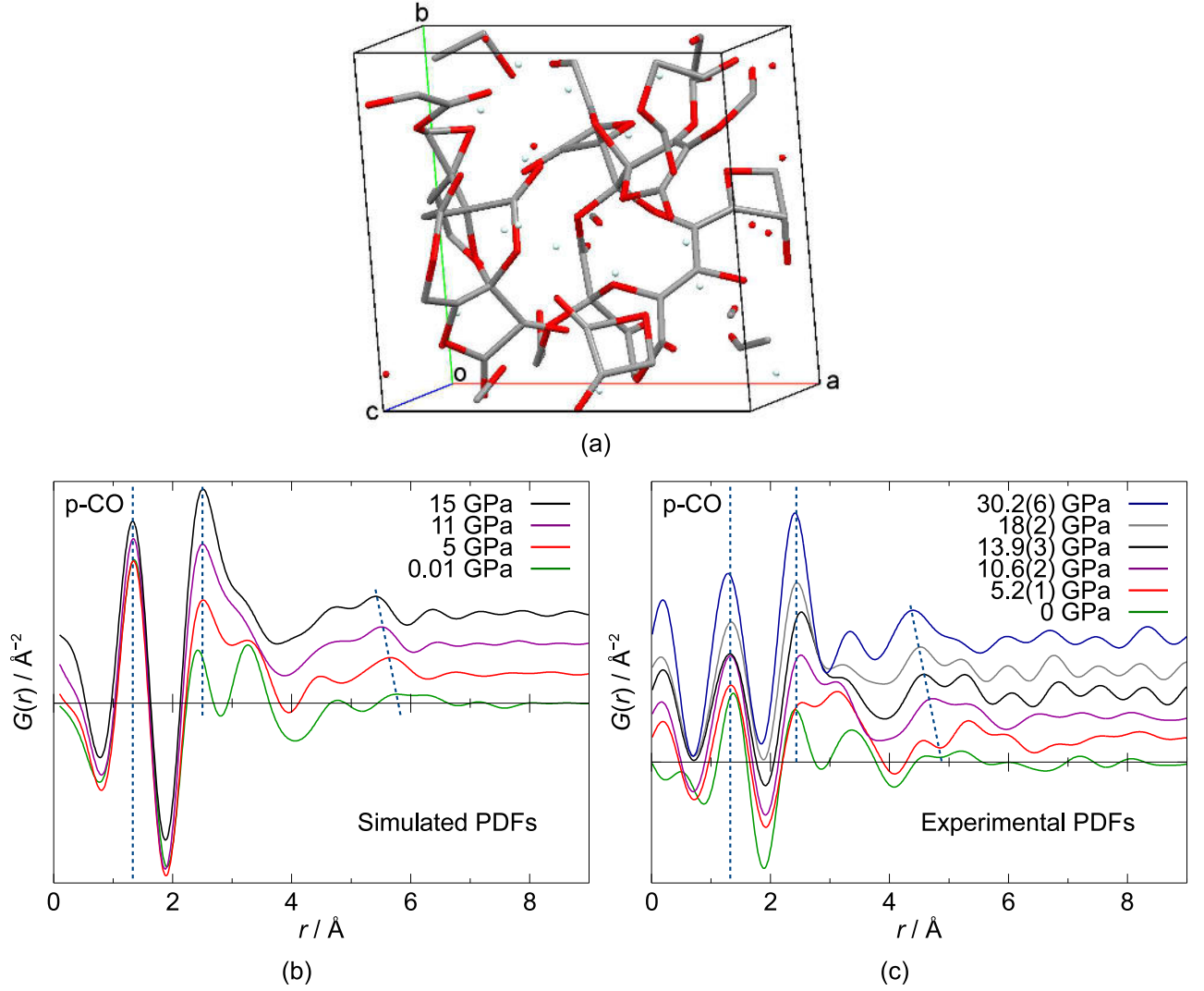


Figure 12: DFT-optimized model of p-CO at 15 GPa (a, C: grey, O: red, He: light blue) and simulated (b) as well as experimental (c) PDFs of p-CO at high pressures (shown with an offset in the ordinate).

3.4 Raman spectroscopy

Figure 14 depicts Raman spectra of liquid CO at 1.9(1) GPa, p-CO at 6.0(1) GPa and recovered p-CO at ambient conditions. The spectrum of liquid CO clearly shows the typical CO band at 2145 cm^{-1} which vanishes in the p-CO spectrum. The positions of the bands in p-CO at around 1600 cm^{-1} and 1800 cm^{-1} are consistent with measurements from Evans et al.^[3] indicating that the p-CO synthesized in this study is similar to the p-CO which has been described earlier. The Raman spectrum of recovered p-CO is also consistent with findings from Evans et al.^[3]. Typical bands of disordered, graphitic carbon are visible at 1356 cm^{-1} and 1585 cm^{-1} (plus overtones).

3.5 Decomposition products of polymerized CO

p-CO was laser heated at 7 to 9 GPa with a pulsed CO_2 laser and at 20(2) GPa with a cw Yb fiber laser resulting in white crystals and black powder, respectively (see figure 5). The large error associated with the nominal pressure of the high pressure experiment is due to

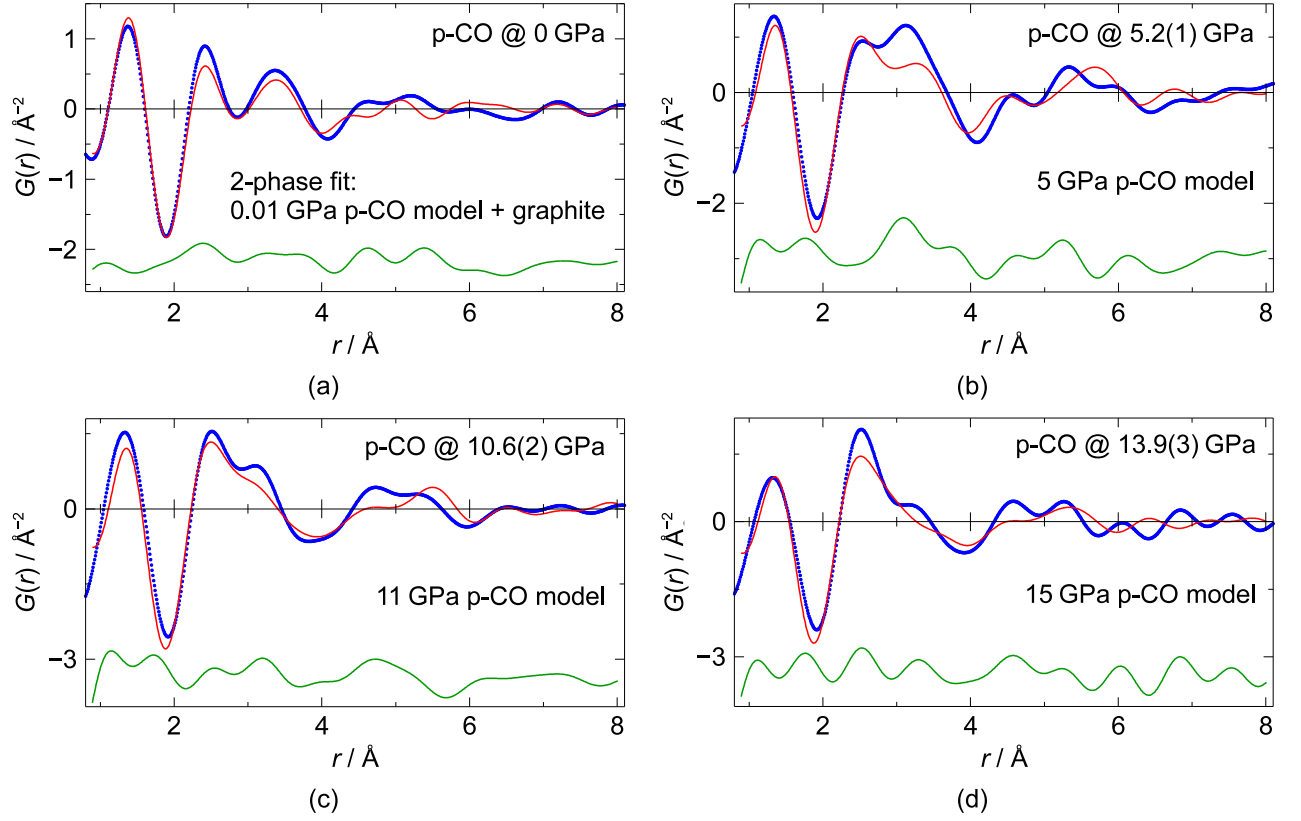


Figure 13: PDF fits of p-CO at different pressures using the DFT-optimized p-CO models. The experimental PDF is shown as blue dotted line in each case, the calculated PDF as red solid line and the difference curve is below in green.

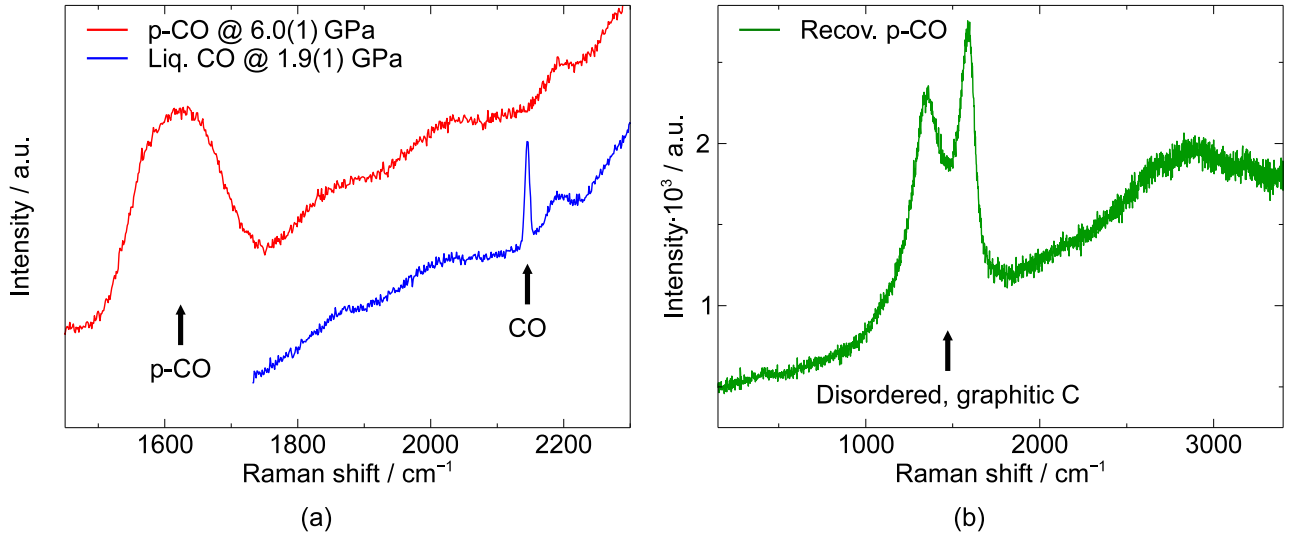


Figure 14: Raman spectra of liquid CO at 1.9 GPa and p-CO at 6 GPa (a) as well as recovered p-CO (b) at ambient conditions.

a significant pressure increase during laser heating. Figure 15 presents the 2D diffraction images before and after laser heating p-CO at 20(2) GPa. Clearly, crystallization was induced by the heating process.

For the white crystals obtained by laser heating at lower pressures, a single crystal

data set was collected at 7.2(1) GPa. 151 reflections were indexed with a cubic unit cell with $a = 5.051(1) \text{ \AA}$, $V = 128.9 \text{ \AA}^3$ and space group $Pa\bar{3}$. This phase corresponds to the known phase CO₂-I and its appearance in our experiments is consistent with the established phase diagram of CO₂^[30] which states that the stable phase at 7 GPa is phase I. Giordano et al.^[30] have determined the volume of CO₂-I to be 130.9 \AA^3 at 7.2 GPa which is in excellent agreement with our value. Our results are also consistent with findings from Evans et al.^[3] who have observed CO₂ bands in Raman spectra taken after laser heating CO at 3 GPa.

Diffraction patterns were also collected for a sample which was laser heated at 20(2) GPa. The stable CO₂ phase at this pressure and ambient temperature is CO₂-III which crystallizes in an orthorhombic lattice with space group $Cmca$ ^[31]. The Le Bail fit is shown in figure 16. Most of the reflections can be described with CO₂-III, W or ruby. The refined lattice parameters result in a volume of $V_{\text{CO}_2} = 26.98(3) \text{ \AA}^3$ per CO₂ molecule. From the equation of state a volume of 27.4 \AA^3 would be expected at around 20 GPa^[32]. This value is in excellent agreement with the results from the Le Bail fit. However, due to the limited quality of the data we could not identify all the reflections in the diffraction pattern.

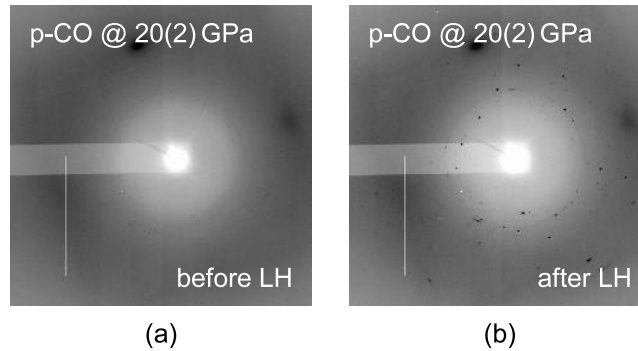


Figure 15: 2D diffraction images of p-CO before (a) and after (b) laser heating at 20(2) GPa.

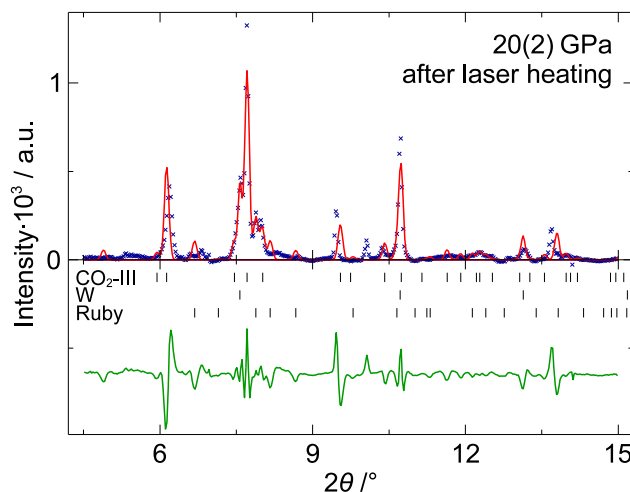


Figure 16: Le Bail fit of the laser heating product of p-CO at 20(2) GPa (blue crosses: data, red line: simulated pattern, green line at the bottom: difference curve, tic marks: calculated reflection positions).

4 Discussion

The comparison of the experimental data obtained from liquid CO at 3.6(2) GPa in our studies and in a previous study by Bellissent-Funel et al.^[12] at 83.5(2) K and $4.2(2) \cdot 10^{-4}$ GPa directly shows the different degrees of compression of liquid CO. The position of the first maximum in the structure function is around $2.25(1) \text{ \AA}^{-1}$ in our study and around 1.9 \AA^{-1} in the previous one. Our experimental PDF shows next neighbors at around 3.5 Å and 6 Å. These values are smaller than the ones obtained by Bellissent-Funel et al.^[12]. This comparison proves that the local structure of the liquid CO at 3.6(2) GPa is compacted compared to the CO which has previously been investigated at low temperatures and pressures which were slightly above ambient pressure. The local structure of liquid CO at 3.6(2) GPa is similar to crystalline analogues. Similar results have been found for example for liquid CS₂, which has a crystal-like local structure at high pressures as well.^[33]

Features in experimental PDFs of p-CO were reproduced with simulated PDFs of DFT-optimized structural models. The structural motifs in the DFT-optimized p-CO showed a wider diversity than the models which have been reported previously^[34] likely due to the larger size of the current model. The types of motifs are consistent with findings from previous studies^[3;4], namely that p-CO consists mostly of long bent chains and to a minor degree of 4- to 6-membered rings (e.g. lactones, cyclic ethers) which are decorated with carbonyl groups.

5 Conclusions

This study presents the determination of the local structures of a liquid CO-rich phase at 3.6(2) GPa and polymerized CO up to 30.2(6) GPa, as well as the identification of its decomposition products by means of X-ray diffraction, including high pressure pair distribution function analysis, single-crystal X-ray diffraction and Raman spectroscopy. DFT calculations provided the corresponding structural models.

The structure of a CO-rich liquid at 3.6(2) GPa was well ordered on a local scale. Simulated PDFs from DFT-optimized crystalline ϵ -CO and δ -CO described the experimental PDF well.

In our experiments, p-CO was observed up to a pressure of 30.2(6) GPa but it began to decompose at around 24 GPa. The pressure-dependent PDFs directly showed the compression of the structure of the network, but the covalent bond lengths did not change. The local atomic arrangement of p-CO was very well reproduced by the models obtained from DFT calculations. These models consisted of a random network of 4-, 5-, and 6-membered cyclic ethers and lactones and carbonyl groups decorating the rings as well as long bent carbon chains with carbonyl groups and bridging atoms. The ring structures were a minor feature in the models.

The decomposition of p-CO induced by laser heating at high pressures resulted in the formation of CO₂ and probably graphitic carbon. The laser-induced decomposition of a quenched sample at ambient conditions yielded disordered, amorphous graphite.

6 Experimental details

A gas mixture of 25 vol% CO in He was obtained from Praxair and loaded without further purification with a gas loading system in Frankfurt. We employed Boehler-Almax^[35] type

diamond anvil cells with opening angles of 48° to 85° . Tungsten gaskets were preindented to thicknesses of 50 to 80 μm and had holes of 120 to 420 μm drilled with a laser lathe (the culet sizes varied between 300 and 800 μm). The pressure was determined with the ruby fluorescence method^[36;37].

The polymerization of CO was induced with a blue 80 mW laser ($\lambda = 473\text{ nm}$, full power) in the laboratory in Frankfurt and with a blue 1 W laser ($\lambda = 457.9\text{ nm}$, $\approx 1.3\%$ power) at the Extreme Conditions Beamline^[38] P02.2, PETRA III, DESY, at 5.3(5) GPa. The error in brackets denotes the range in which the polymerization was observed in several experiments. The uncertainty of the pressure measurement is about 2% or at least 0.1 GPa. The blue 80 mW laser was also used to measure Raman spectra of liquid CO as well as p-CO in the DAC. Additional micro-Raman experiments of p-CO and p-CO recovered at ambient conditions were carried out using a Renishaw spectrometer (RM-1000) and a CCD detector with a Nd:YAG laser ($\lambda = 532\text{ nm}$). One-sided laser heating of p-CO at around 7 GPa was performed in our laboratory with a 250 W pulsed CO₂ laser ($\lambda = 10.6\text{ }\mu\text{m}$)^[39] and during diffraction experiments at 20(2) GPa at P02.2 with a 100 W Yb fiber laser ($\lambda = 1070\text{ nm}$). p-CO decomposed immediately at the lowest laser powers and hence temperature measurements were impossible.

Synchrotron X-ray diffraction experiments were performed in different beam times at P02.2 of the PETRA III facility at DESY. We used 42.4 to 42.8 keV radiation (λ : 0.293 to 0.290 \AA). The beam was focused to around $2\text{ }\mu\text{m} \times 2\text{ }\mu\text{m}$ (FWHM) with Kirkpatrick-Baez mirrors or $10\text{ }\mu\text{m} \times 10\text{ }\mu\text{m}$ (FWHM) with a compound refractive lens system. Diffractograms suitable for PDF analysis as well as single crystal data (ω scan, step size 1°) were measured. The diffraction data were collected with a PerkinElmer XRD 1621 detector and the single crystal data with a MAR345 image plate. Sample-detector distances varied between 310 mm for the PDF measurements and 400 to 500 mm for the other diffraction and single crystal data. The data collection times varied between 10 s per frame for the single crystal data and up to 10 min per frame for the PDF data.

X-ray diffraction data of liquid CO were collected at a pressure of 3.6(2) GPa, of p-CO at numerous pressures ranging from 4.8 to 30 GPa, of the products after laser heating at 7 to 9 GPa and 20(2) GPa and of several p-CO samples recovered at ambient conditions. Due to the small beam size and the separation of the CO and the He, it was possible to perform the sample and the background measurement, which is important for the PDF analysis, in one DAC only at the same pressure. Thus, there was no need to reload the DAC with the pressure medium only and remeasure every pressure step to obtain the background measurement for the PDF analysis.

The diffraction data were processed using the *Fit2D* software^[40]. A CeO₂ standard was used for calibration. PDFs were obtained by a Fourier transform of the corrected and normalized diffraction patterns using standard procedures and those unique to area detectors implemented in the program *PDFgetX2*^[41] and which are described in Chupas et al.^[42]. Depending on the data quality, the diffractograms were terminated at Q_{max} between 9 and 12 \AA^{-1} . In some cases it was necessary to remove reflections from the tungsten gasket manually before the data were processed. PDF simulations and refinements were performed with the *PDFgui* program^[43]. The atomic positions, unit cell parameters, isotropic displacement parameters ($u_{\text{iso}} = 0.005\text{ \AA}^2$) and δ_2 (δ_2 : 0–1.5) were fixed during the refinements. A scaling factor and Q_{damp} were refined. Le Bail fits were performed using the programs *GSAS*^[44] and *EXPGUI*^[45]. The background was interpolated using a shifted Chebyshev function between manually defined points, and profile parameters and unit cell parameters were refined. The single crystal data were indexed and reduced with

the program *CrysAlis* version 171.33.41 (Agilent Technologies).

7 Acknowledgment

The authors gratefully acknowledge financial support by the BMBF (projects 05K10RFA and 05K13RF1), the DFG (project WI1232/25-1), the US Army Research Office (contract W911NF-12-2-0063) and the International Centre of Diffraction Data. The authors acknowledge Prof. Dr. A. Woodland for access to the micro-Raman spectrometer and Prof. Dr. L. Ehm for helpful discussions. Part of the research was carried out at the light source PETRA III at DESY, a member of the Helmholtz Association HGF. We thank the beamline scientist of P02.2, H.-P. Liermann, and his team.

References

- [1] V. Schettino and R. Bini. Molecules under extreme conditions: Chemical reactions at high pressure. *Phys. Chem. Chem. Phys.*, 5:1951–1965, 2003.
- [2] R. Bini, M. Ceppatelli, M. Citroni, and V. Schettino. From simple to complex and backwards. Chemical reactions under very high pressure. *Chem. Phys.*, 398:262–268, 2012.
- [3] W. J. Evans, M. J. Lipp, C.-S. Yoo, H. Cynn, J. L. Herberg, R. S. Maxwell, and M. F. Nicol. Pressure-Induced Polymerization of Carbon Monoxide: Disproportionation and Synthesis of an Energetic Lactonic Polymer. *Chem. Mater.*, 18:2520–2531, 2006.
- [4] M. Ceppatelli, A. Serdyukov, R. Bini, and H. J. Jodl. Pressure Induced Reactivity of Solid CO by FTIR Studies. *J. Phys. Chem. B*, 113:6652–6660, 2009.
- [5] V. Iota, C. S. Yoo, and H. Cynn. Quartzlike Carbon Dioxide: An Optically Nonlinear Extended Solid at High Pressures and Temperatures. *Science*, 283:1510–1513, 1999.
- [6] A. I. Katz, D. Schiferl, and R. L. Mills. New Phases and Chemical Reactions in Solid CO under Pressure. *J. Phys. Chem.*, 88:3176–3179, 1984.
- [7] R. L. Mills, D. Schiferl, A. I. Katz, and B. W. Olinger. New Phases and Chemical Reactions in Solid CO Under Pressure. *J. Phys. (Paris) Colloques C*, 45:8–187, 1984.
- [8] M. J. Lipp, W. J. Evans, B. J. Baer, and C.-S. Yoo. High-energy-density extended CO solid. *Nat. Mater.*, 4:211–215, 2005.
- [9] R. L. Mills, B. Olinger, and D. T. Cromer. Structures and phase diagrams of N₂ and CO to 13 GPa by x-ray diffraction. *J. Chem. Phys.*, 84:2837–2845, 1986.
- [10] M. Lipp, W. J. Evans, V. Garcia-Baonza, and H. E. Lorenzana. Carbon Monoxide: Spectroscopic Characterization of the High-Pressure Polymerized Phase. *J. Low Temp. Phys.*, 111:247–256, 1998.
- [11] M. A. Howe, C. J. Wormald, and G. W. Neilson. The structure of the molecular liquids carbon monoxide (CO) and nitric oxide (NO) as determined by neutron scattering. *Mol. Phys.*, 66:847–858, 1989.

- [12] M.-C. Bellissent-Funel, U. Buontempo, C. Petrillo, and F. P. Ricci. Orientational correlations in liquid CO: neutron-diffraction measurements. *Mol. Phys.*, 71:239–251, 1990.
- [13] L. Temleitner and L. Pusztai. Orientational correlations in liquid carbon monoxide and nitric oxide. *J. Phys.: Condens. Matter*, 17:S47–S57, 2005.
- [14] T. Proffen and H. Kim. Advances in total scattering analysis. *J. Mater. Chem.*, 19:5078–5088, 2009.
- [15] S. J. L. Billinge and M. G. Kanatzidis. Beyond crystallography: the study of disorder, nanocrystallinity and crystallographically challenged materials with pair distribution functions. *Chem. Commun.*, 7:749–760, 2004.
- [16] K. W. Chapman, P. J. Chupas, G. J. Halder, J. A. Hriljac, C. Kurtz, B. K. Greve, C. J. Ruschman, and A. P. Wilkinson. Optimizing high-pressure pair distribution function measurements in diamond anvil cells. *J. Appl. Cryst.*, 43:297–307, 2010.
- [17] L. Ehm, L. A. Borkowski, J. B. Parise, S. Ghose, and Z. Chen. Evidence of tetragonal nanodomains in the high-pressure polymorph of BaTiO₃. *Appl. Phys. Lett.*, 98:021901, 2011.
- [18] T. Egami and S. J. L. Billinge. *Underneath the Bragg Peaks – Structural Analysis of Complex Materials*. Pergamon, 2003.
- [19] X. Gonze and C. Lee. Dynamical matrices, Born effective charges, dielectric permittivity tensors, and interatomic force constants from density-functional perturbation theory. *Phys. Rev. B*, 55:10355–10368, 1997.
- [20] S. Clark, M. Segall, C. Pickard, P. Hasnip, M. Probert, K. Refson, and M. Payne. First principles methods using CASTEP. *Z. Kristallogr.*, 220:567–570, 2005.
- [21] J. P. Perdew, A. Ruzsinszky, G. I. Csonka, O. A. Vydrov, G. E. Scuseria, L. A. Constantin, X. Zhou, and K. Burke. Restoring the Density-Gradient Expansion for Exchange in Solids and Surfaces. *Phys. Rev. Lett.*, 100:136406, 2008.
- [22] H. J. Monkhorst and J. D. Pack. Special points for Brillouin-zone integrations. *Phys. Rev. B*, 13:5188–5192, 1976.
- [23] L. Vegard. Struktur und Leuchtfähigkeit von festem Kohlenoxyd. *Z. Phys.*, 61:185–190, 1930.
- [24] J. VandeVondele, M. Krack, F. Mohamed, M. Parrinello, T. Chassaing, and Jürg Hutter. QUICKSTEP: Fast and accurate density functional calculations using a mixed Gaussian and plane waves approach. *Comput. Phys. Commun.*, 167:103–128, 2005.
- [25] S. Goedecker, M. Teter, and J. Hutter. Separable dual-space Gaussian pseudopotentials. *Phys. Rev. B*, 54:1703–1710, 1996.
- [26] C. Hartwigsen, S. Goedecker, and J. Hutter. Relativistic separable dual-space Gaussian pseudopotentials from H to Rn. *Phys. Rev. B*, 58:3641–3662, 1998.

- [27] S. Grimme, J. Antony, S. Ehrlich, and H. Krieg. A consistent and accurate *ab initio* parameterization of density functional dispersion correction (DFT-D) for the 94 elements H–Pu. *J. Chem. Phys.*, 132:154104, 2010.
- [28] I. G. Batyrev, W. D. Mattson, and B. M. Rice. Modeling of a random network of extended CO solids. *AIP Conf. Proc.*, 1426:717–720, 2012.
- [29] D. T. Cromer, D. Schiferl, R. LeSar, and R. L. Mills. Room-temperature structure of carbon monoxide at 2.7 and 3.6 GPa. *Acta. Cryst.*, C39:1146–1150, 1983.
- [30] V. M. Giordano, F. Datchi, F. A. Gorelli, and R. Bini. Equation of state and anharmonicity of carbon dioxide phase I up to 12 GPa and 800 K. *J. Chem. Phys.*, 133:144501, 2010.
- [31] K. Aoki, H. Yamawaki, M. Sakashita, Y. Gotoh, and K. Takemura. Crystal Structure of the High-Pressure Phase of Solid CO₂. *Science*, 263:356–358, 1994.
- [32] M. Santoro and F. A. Gorelli. High pressure solid state chemistry of carbon dioxide. *Chem. Soc. Rev.*, 35:918–931, 2006.
- [33] S. Yamamoto, Y. Ishibashi, Y. Inamura, Y. Katayama, T. Mishina, and J. Nakahara. Pressure dependence of local structure in liquid carbon disulfide. *J. Chem. Phys.*, 124:144511, 2006.
- [34] S. Bernard, G. L. Chiarotti, S. Scandolo, and E. Tosatti. Decomposition and Polymerization of Solid Carbon Monoxide under Pressure. *Phys. Rev. Lett.*, 81:2092–2095, 1998.
- [35] R. Boehler. New diamond cell for single-crystal x-ray diffraction. *Rev. Sci. Instrum.*, 77:115103, 2006.
- [36] H. K. Mao, P. M. Bell, J. W. Shaner, and D. J. Steinberg. Specific volume measurements of Cu, Mo, Pd, and Ag and calibration of the ruby R_1 fluorescence pressure gauge from 0.06 to 1 Mbar. *J. Appl. Phys.*, 49:3276–3283, 1978.
- [37] H. K. Mao, J. Xu, and P. M. Bell. Calibration of the Ruby Pressure Gauge to 800 kbar Under Quasi-Hydrostatic Conditions. *J. Geophys. Res.*, 91:4673–4676, 1986.
- [38] H.-P. Liermann, W. Morgenroth, A. Ehnes, A. Berghäuser, B. Winkler, H. Franz, and E. Weckert. The Extreme Conditions Beamline at PETRA III, DESY: Possibilities to conduct time resolved monochromatic diffraction experiments in dynamic and laser heated DAC. *J. Phys. Conf. Ser.*, 215:012029, 2010.
- [39] L. Bayarjargal, T. G. Shumilova, A. Friedrich, and B. Winkler. Diamond formation from CaCO₃ at high pressure and temperature. *Eur. J. Mineral.*, 22:29–34, 2010.
- [40] A. P. Hammersley, S. O. Svensson, M. Hanfland, A. N. Fitch, and D. Häusermann. Two-dimensional detector software: From real detector to idealised image or two-theta scan. *High Press. Res.*, 14:235–248, 1996.
- [41] X. Qiu, J. W. Thompson, and S. J. L. Billinge. PDFgetX2: a GUI-driven program to obtain the pair distribution function from X-ray powder diffraction data. *J. Appl. Cryst.*, 37:678, 2004.

- [42] P. J. Chupas, X. Qiu, J. C. Hanson, P. L. Lee, C. P. Grey, and S. J. L. Billinge. Rapid-acquisition pair distribution function (RA-PDF) analysis. *J. Appl. Cryst.*, 36: 1342–1347, 2003.
- [43] C. L. Farrow, P. Juhas, J. W. Liu, D. Bryndin, E. S. Božin, J. Bloch, Th. Proffen, and S. J. L. Billinge. PDFfit2 and PDFgui: computer programs for studying nanostructure in crystals. *J. Phys.: Condens. Matter*, 19:335219, 2007.
- [44] A. C. Larson and R. B. von Dreele. General Structure Analysis System (GSAS). Los Alamos National Laboratory Report LAUR 86-748, 2004.
- [45] B. H. Toby. *EXPGUI*, a graphical user interface for *GSAS*. *J. Appl. Cryst.*, 34: 210–213, 2001.

Graphical abstract:

The local atomic structures of liquid and polymerized CO (p-CO) and its decomposition products have been analyzed at pressures up to 30 GPa in diamond anvil cells using high pressure pair distribution function (PDF) analysis. The PDF of liquid CO is very distinct from the PDF of polymerized CO (see picture). The local structures of liquid CO and polymerized CO were explained using simulations from DFT-optimized structural models.

